Ocean Engineering 245 (2022) 110327

Contents lists available at ScienceDirect

Ocean Engineering

journal homepage: www.elsevier.com/locate/oceaneng

Wave diffraction from an array of porous cylinders with porous plates fixed inside

GuangYuan Wang [a,c], MoHan Zhang [b,d,*], HuaQing Zhang [a,c], FaJun Yu [e]

[a] College of River and Ocean Engineering, Chongqing Jiaotong University, Chongqing, 400074, China
[b] School of Engineering Science, University of Chinese Academy of Sciences, Beijing, 100049, China
[c] Tianjin Research Institute for Water Transport Engineering, M.O.T., Tianjin, 300000, China
[d] Key Laboratory for Mechanics in Fluid Solid Coupling Systems, Institute of Mechanics, Chinese Academy of Sciences, Beijing, 100190, China
[e] College of Shipbuilding Engineering, Harbin Engineering University, Harbin, 150001, China

ARTICLE INFO

Keywords:
Porous cylinders
Porous plates
Wave diffraction
Eigenfunction expansion

ABSTRACT

The interaction between water wave and an array of porous cylinders with porous plates fixed inside is investigated theoretically in this study. The porous cylinders are bottom-mounted and surface-piercing, which contain porous plates fixed below the free water surface. The analytical solution of velocity potential in the flow field is derived using eigenfunction expansion and Graf's addition theorem for Bessel functions under the assumptions of potential flow theory and linear wave theory. This paper focus on investigating the influence of the porous plates on the diffraction process of the multiple porous cylinders. The results show that the existence of the porous plates has little effect on the surge force of the porous cylinders, but it can reduce the wave run up inside the cylinders. The behavior of the porous plates and porous cylinders in combination is similar to that of a wave absorber, which may cause a setdown of the free surface elevation on the array's downstream side.

1. Introduction

The viability of traditional impermeable structures has been severely threatened by the enormous hydrodynamic loads as marine engineering structures such as offshore platforms and offshore wind turbines have been developed into deeper waters. Dissipation of wave energy is an effective means of reducing hydrodynamic loads on structures. Extensive studies have shown that porous structures can act as wave absorbers. Therefore, porous structures, especially porous cylinders, have attracted great interest from researchers.

Wang and Ren (1994) was the first to study the protective effect of the porous outer cylinder on the impermeable inner cylinder. Darwiche et al. (1994) extended the work to a semi-porous cylindrical breakwater, and Williams and Li (1998) extended it to a semi-porous cylindrical breakwater installed on a storage tank.

Early studies were limited to the isolated porous cylinder, while studies for the array of cylinders focused more on impermeable cylinders. The analytical solution between the array of cylinders and waves was originally proposed by Spring and Monkmeyer (1974). They investigated the interaction of an array of bottom-mounted, surface-piercing, impermeable cylinders with waves using the eigenfunction expansion approach and Graf's addition theory for Bessel functions. Later, Linton and Evans (1990) simplified the method. Since then, many scholars (Maniar and Newman, 1997; Walker and Taylor, 2005; Zeng et al., 2019) have used this method to study the interaction between waves and the array of impermeable cylinders. Few studies have investigated the array of porous cylinders. Williams and Li (2000) obtained the diffraction analytical solution of waves and an array of porous cylinders by the above method. They found that the permeability of the structure can effectively reduce the hydrodynamic force and wave run up of the cylinders. Sankarbabu et al. (2007) continued to use this method to extend the concentric porous cylinder system studied by Wang and Ren (1994) to an array of concentric porous cylinders.

On the other hand, many scholars have recognized porous plates with wave dissipation capability as a promising marine structure. The interaction between a submerged porous plate and water wave was first investigated theoretically by Chwang and Wu (1994). Eigenfunction expansion and Darcy's law were used to derive the velocity potential in the flow field. Their results show that the porous plate acts as a wave absorber. Since then, many scholars (Yip and Chwang, 1998; Cho and Kim, 2000, 2008; Liu et al., 2007, 2008) have conducted extensive research on different types of porous plates. All of the above studies require the solution of complex eigenvalues, which can be troublesome

* Corresponding author at: School of Engineering Science, University of Chinese Academy of Sciences, Beijing, 100049, China.
E-mail address: zmh_imech@163.com (M. Zhang).

https://doi.org/10.1016/j.oceaneng.2021.110327
Received 10 September 2021; Received in revised form 29 November 2021; Accepted 4 December 2021
Available online 5 January 2022

under certain parameter conditions. To circumvent this trouble, many academics (Molin et al., 2004; Evans and Peter, 2011; Liu and Li, 2011; Liu et al., 2011; Cho and Kim, 2013; Zhao et al., 2017) have devised other approaches to divide the vertical space into two independent regions. It is found that both of the methods are effective in tackling the problem of the porous plate and wave interaction.

Based on the rich research results of the porous cylinder and porous plate, the combined application of both has also been considered by scholars to optimize the hydrodynamic performance of the structure. Wu and Chwang (2002) studied a vertical cylinder with a porous ring plate. They found that the presence of a porous ring plate not only reduces the wave run up at the front edge of the cylinder, but also reduces the hydrodynamic loads on the cylinder. Bao et al. (2009) and Zhao et al. (2010) investigated the water wave interaction with a cylinder with a horizontal porous plate fixed inside theoretically and verified it experimentally. Recently, Wang et al. (2021) extended the study to a concentric two cylinders system with a plate fixed inside. These studies clearly indicate that the combined application of porous plates and porous cylinders is expected to achieve better hydrodynamic performance.

So far, no systematic analysis of diffraction from porous cylindrical arrays with porous plates fixed inside has been performed. The influence of the porous plates on the array of porous cylinders has remained unclear. The primary aim of this paper is to evaluate the effect of the porous plates on the diffraction process of the array of porous cylinders. The porous cylinders are bottom-mounted and surface-piercing. The porous plates are considered to be thin and fixed below the still water surface. Based on the eigenfunction expansion approach, analytical solutions of the velocity potential in each of the regions are derived under the assumptions of linearized potential flow. The diffraction processes of an isolated cylinder and a four-cylinders system with varying wave and structural parameters are explored using this analytical solution. The array of porous cylinders with porous plates fixed inside can be used not only as a breakwater, but also as a support component for marine structures. The research results of this paper are instructive for their engineering applications.

The mathematical model, including governing equations and boundary conditions, are presented in Section 2. The analytical solution is derived in Section 3. The validations and some numerical results are given in Section 4. The last section is the conclusion of this paper.

2. Theoretical development

Fig. 1 shows a definition sketch of an arbitrary array of N bottom-mounted cylinders with porous plates fixed inside. Symbol a and d represent the radius and draft of the plates, respectively. Symbol h is the water depth. With the origin at still water level and z pointing vertically upwards, the global coordinates (x, y, z) are established. Fig. 1 depicts the various parameters relating to the positions of the N cylinders. The origin of the local polar coordinate system (r_j, θ_j) is located at the center of cylinder j, with $j = 1, 2, \ldots, N$, where θ_j is measured counterclockwise from the positive x-axis. The center of cylinder k has polar coordinates (R_{kj}, α_{kj}) relative to cylinder j, where $j, k = 1, 2, \ldots, N$. The array of cylinders is subjected to regular wave of amplitude, A and angular frequency, ω propagating at an angle, β to the positive x-axis. Considering the fluid to be inviscid and incompressible, and the flow to be irrotational, the flow can be described in the fluid domain by a velocity potential $\Phi(x, y, z, t)$ satisfying Laplace's equation. The motion is assumed time harmonic with angular frequency, so the velocity potential can be written as:

$$\Phi(x, y, z, t) = \mathrm{Re}\left[\phi(x, y, z)\, e^{-\mathrm{i}\omega t}\right] \tag{1}$$

where Re represents the real part of the complex expression, ϕ the spatial velocity potential, i the imaginary unit, ω the angular frequency of the incident wave.

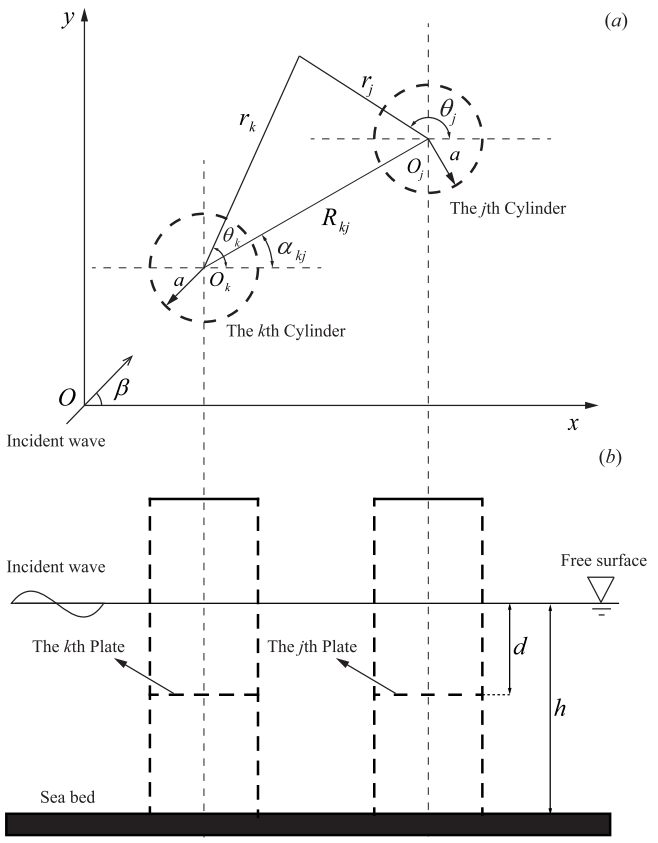

Fig. 1. Definition sketch.

The fluid is divided into $N + 1$ regions, with N interior regions $(0 \le r_j \le a,\ j = 1, 2, \ldots, N)$ in the vertical space of N cylinders and an exterior region $(a < r_j,\ j = 1, 2, \ldots, N)$. In these regions, the velocity potentials will be symbolized by $\phi_0(x, y, z)$ and $\phi_j(x, y, z)$, $j = 1, 2, \ldots, N$, respectively, and must satisfy the Laplace's equation:

$$\nabla^2 \phi_j(x, y) = 0,\ j = 0, 1, 2, \ldots, N. \tag{2}$$

The velocity potential of each region also satisfies the conditions of free surface and seafloor, i.e.

$$\frac{\partial \phi_j}{\partial z} = \frac{\omega^2}{g}\phi_j,\ z = 0,\quad j = 0, 1, 2, \ldots, N, \tag{3}$$

$$\frac{\partial \phi_j}{\partial z} = 0,\ z = -h,\ j = 0, 1, 2, \ldots, N. \tag{4}$$

On the porous plates and cylinders, the boundary conditions can be expressed as:

$$\frac{\partial \phi_j}{\partial z}\Big|_{z=-d^+} = \frac{\partial \phi_j}{\partial z}\Big|_{z=-d^-} = -w_j^d(\theta, r),\ j = 1, 2, \ldots, N, \tag{5}$$

$$\frac{\partial \phi_0}{\partial r}\Big|_{r=a^+} = \frac{\partial \phi_j}{\partial r}\Big|_{r=a^-} = -w_j^a(\theta, z),\ j = 1, 2, \ldots, N, \tag{6}$$

where $w_j^d(\theta, r)$ and $w_j^a(\theta, z)$ are the spatial component of $W_j^d(\theta, r, t)$ and $W_j^a(\theta, z, t)$, which are the flow velocity passing through the porous plates and porous cylinders, respectively. The plus and minus signs in Eq. (5) represent the upper and lower surfaces of the plates, respectively. The plus and minus signs in Eq. (6) represent the outer and inner surfaces of the cylinders, respectively. Our investigation is limited to porous surfaces with fine pores. Darcy's law can be considered to apply to fluid flow through the porous surfaces. Therefore, the flow velocity is linearly proportional to the pressure difference between the

two sides of the porous surfaces (Taylor, 1956; Wang and Ren, 1994). We have:

$$W_j^d(\theta,r,t)=\frac{l_0}{\mu}\left(P_j\mid_{z=-d^+}-P_j\mid_{z=-d^-}\right),\ j=1,\ 2,\ldots,\ N, \tag{7}$$

$$W_j^a(\theta,z,t)=\frac{l_1}{\mu}\left(P_0\mid_{r=a^+}-P_j\mid_{r=a^-}\right),\ j=1,\ 2,\ldots,\ N. \tag{8}$$

Here, μ is the constant coefficient of dynamic viscosity. $l_q\,(q=0,\ 1)$ represent material constants of the plates and cylinders respectively, both of which having the dimension of a length. $P_j\,(j=1,\ 2,\ldots,\ N)$ is the hydrodynamic pressure on cylinder j, which can be derived by the velocity potentials through the linearized Bernoulli equation:

$$P_j=-\rho\frac{\partial \boldsymbol{\Phi}_j}{\partial t},\ j=0,\ 1,\ 2,\ldots,\ N, \tag{9}$$

where ρ is the constant fluid density. We can get the expression for w_j^d and w_j^a by substituting formula (9) into formula (7) and (8):

$$w_j^d(r,\ \theta)=\frac{\mathrm{i}\rho\omega l_0}{\mu}\left[\phi_j\left(r,\theta,-d^+\right)-\phi_j\left(r,\theta,-d^-\right)\right],\ j=0,\ 1,\ 2,\ldots,\ N, \tag{10}$$

$$w_j^b(\theta,\ z)=\frac{\mathrm{i}\rho\omega l_1}{\mu}\left[\phi_0\left(a^+,\ \theta,\ z\right)-\phi_j\left(a^-,\ \theta,\ z\right)\right],\ j=1,\ 2,\ldots,\ N. \tag{11}$$

Substituting (10) into (5), we can get:

$$\frac{\partial\phi_j}{\partial z}\mid_{z=-d^+}=\frac{\partial\phi_j}{\partial z}\mid_{z=-d^-}=-\frac{\mathrm{i}\rho\omega l_0}{\mu}\left[\phi_j\left(r,\theta,-d^+\right)-\phi_j\left(r,\theta,-d^-\right)\right],\quad j=1,\ 2,\ldots,\ N. \tag{12}$$

Similarly, substituting (11) into (6), we can get:

$$\frac{\partial\phi_0}{\partial r}\mid_{r=a^+}=\frac{\partial\phi_j}{\partial r}\mid_{r=a^-}=-\frac{\mathrm{i}\rho\omega l_1}{\mu}\left[\phi_0\left(a^+,\ \theta,\ z\right)-\phi_j\left(a^-,\ \theta,\ z\right)\right],\quad j=1,\ 2,\ldots,\ N. \tag{13}$$

Define the porous effect parameters $\sigma_n=\rho\omega l_n/\mu\ \ (n=0,\ 1)$, where $n=0$ and 1 represent the porous effect parameters of the plates and cylinders, respectively, we have:

$$\frac{\partial\phi_j}{\partial z}\mid_{z=-d^+}=\frac{\partial\phi_j}{\partial z}\mid_{z=-d^-}=\mathrm{i}\sigma_0\left[\phi_j\left(r,\theta,-d^-\right)-\phi_j\left(r,\theta,-d^+\right)\right],\quad j=1,\ 2,\ldots,\ N. \tag{14}$$

$$\frac{\partial\phi_0}{\partial r}\mid_{r=a^+}=\frac{\partial\phi_j}{\partial r}\mid_{r=a^-}=\mathrm{i}\sigma_1\left[\phi_j\left(a^-,\ \theta,\ z\right)-\phi_0\left(a^+,\ \theta,\ z\right)\right],\quad j=1,\ 2,\ldots,\ N. \tag{15}$$

The dimensionless porous effect parameter b_n is further introduced:

$$b_n=\frac{2\pi\sigma_n}{k_0},\ n=0,\ 1. \tag{16}$$

Furthermore, the diffraction component of the exterior region velocity potential must satisfy the Sommerfeld condition:

$$\lim_{r\to\infty}\sqrt{r}\left[\frac{\partial}{\partial r}\left(\phi_0-\phi_I\right)-\mathrm{i}k_0\left(\phi_0-\phi_I\right)\right]=0, \tag{17}$$

where ϕ_I is the incident velocity potential.

The velocity potentials on the common boundaries between different regions must satisfy the following transmission conditions:

$$\frac{\partial\phi_0}{\partial r}=\frac{\partial\phi_k}{\partial r},\quad k=1,2,\ldots,\ N,\ r_k=a,-h<z<0, \tag{18}$$

$$\phi_0=\phi_k-\frac{1}{\mathrm{i}\sigma_1}\frac{\partial\phi_k}{\partial r},\ k=1,\ 2,\ldots,\ N,\ r_k=a,\ -h<z<0. \tag{19}$$

3. Solution to the problem

The incident potential in the jth polar coordinate system, can be expressed as:

$$\phi_I^j\left(r_j,\theta_j,z_j\right)=\frac{-\mathrm{i}gA}{\omega}\frac{\cosh\left[k_0\left(z_j+h\right)\right]}{\cosh\left(k_0h\right)}I_j\sum_{n=-\infty}^{\infty}J_n\left(k_0r_j\right)e^{\mathrm{i}n\left(\pi/2-\beta+\theta_j\right)}, \tag{20}$$

where $I_j=e^{\mathrm{i}\left(x_j\cos\beta+y_j\sin\beta\right)}$ is the phase vector corresponding to the jth cylinder. J_n represents the Bessel function of the first kind with order n. β and k_0 are the direction and wavenumber of the incident wave.

The wave diffracted by cylinder j in the array of cylinders can be expressed as:

$$\phi_D^j\left(r_j,\theta_j,z_j\right)=\sum_{n=-\infty}^{\infty}e^{\mathrm{i}n\theta_j}\left[\sum_{p=0}^{\infty}A_{np}^jR_n\left(k_pr_j\right)Z_p\left(k_pz_j\right)\right], \tag{21}$$

where A_{np}^j are the unknown complex coefficients.

The radial eigenfunctions $R_n\left(k_pr\right)$ and vertical eigenfunctions $Z_p\left(k_pz\right)$ are given as:

$$R_n\left(k_pr\right)=\begin{cases}H_n\left(k_0r\right), & p=0\\ K_n\left(k_pr\right), & p\geq 1\end{cases},$$

$$Z_p\left(k_pz\right)=\begin{cases}\frac{-\mathrm{i}gA}{\omega}\frac{\cosh\left[k_0(z+h)\right]}{\cosh\left(k_0h\right)}, & p=0\\ \frac{-\mathrm{i}gA}{\omega}\frac{\cos\left[k_p(z+h)\right]}{\cos\left(k_ph\right)}, & p\geq 1\end{cases}.$$

Here, H_n is the first kind of Hankel function with order n, and K_n denotes the second kind modified Bessel function with order n. k_p are the positive real roots of the dispersion relation as follows:

$$-k\tan\left(kh\right)=\frac{\omega^2}{g}.$$

The total velocity potential near cylinder j is given by:

$$\begin{aligned}\phi_0\left(r_j,\theta_j,z_j\right)=&I_j\sum_{n=-\infty}^{\infty}J_n\left(k_0r_j\right)e^{\mathrm{i}n\left(\frac{\pi}{2}-\beta+\theta_j\right)}Z_0\left(k_0z_j\right)\\&+\sum_{j=1}^{N}\sum_{n=-\infty}^{\infty}e^{\mathrm{i}n\theta_j}\left[\sum_{p=0}^{\infty}A_{np}^jR_n\left(k_pr_j\right)Z_p\left(k_pz_j\right)\right].\end{aligned} \tag{22}$$

The second term on the right side of formula (22) can be expressed using Graf's addition theorem for Bessel functions (Abramowitz and Stegun, 1964; Kagemoto and Yue, 1986) as

$$\sum_{j=1}^{N}\sum_{n=-\infty}^{\infty}\sum_{p=0}^{\infty}A_{np}^jZ_p\left(k_pz_j\right)\sum_{m=-\infty}^{\infty}Q_{n,m}^{j,k}\left(k_pr_k\right)e^{-\mathrm{i}m\theta_k}, \tag{23}$$

where

$$Q_{n,m}^{j,k}\left(k_pr_k\right)=\begin{cases}H_{n+m}\left(k_0R_{jk}\right)J_m\left(k_0r_k\right)e^{\mathrm{i}(m+n)\alpha_{jk}}e^{\mathrm{i}m\pi}, & p=0\\ K_{n+m}\left(k_pR_{jk}\right)I_m\left(k_pr_k\right)e^{\mathrm{i}(m+n)\alpha_{jk}}e^{\mathrm{i}m\pi}, & p\geq 1\end{cases}.$$

Replace m in (23) with $-m$, we can get:

$$\begin{aligned}\phi_0\left(r_k,\theta_k,z_k\right)=&\sum_{n=-\infty}^{\infty}e^{\mathrm{i}n\theta_k}\left[I_kJ_n\left(k_0r_k\right)e^{\mathrm{i}n\left(\frac{\pi}{2}-\beta\right)}Z_0\left(k_0z_k\right)\right.\\&\left.+\sum_{p=0}^{\infty}A_{np}^kR_n\left(k_pr_k\right)Z_p\left(k_pz_k\right)\right]\\&+\sum_{j=1,j\neq k}^{N}\sum_{n=-\infty}^{\infty}\sum_{p=0}^{\infty}A_{np}^jZ_p\left(k_pz_j\right)\sum_{m=-\infty}^{\infty}Q_{n,-m}^{jk}\left(k_pr_k\right)e^{\mathrm{i}m\theta_k},\end{aligned} \tag{24}$$

where

$$Q_{n,-m}^{j,k}\left(k_pr_k\right)=\begin{cases}H_{n-m}\left(k_0R_{jk}\right)J_m\left(k_0r_k\right)e^{\mathrm{i}(n-m)\alpha_{jk}}, & p=0\\ K_{n-m}\left(k_pR_{jk}\right)I_m\left(k_pr_k\right)e^{\mathrm{i}(n-m)\alpha_{jk}}(-1)^m, & p\geq 1\end{cases}.$$

The potential $\phi_k\ (k = 1,\ 2, \ldots,\ N)$ of the kth interior region, can be expressed as follows:

$$\phi_k\left(r_k, \theta_k, z_k\right) = \sum_{n=-\infty}^{\infty} e^{\mathrm{i}n\theta_k} \sum_{l=1}^{\infty} D_{nl}^k \frac{J_n\left(\kappa_l r_k\right)}{J_n\left(\kappa_l a\right)} T_l\left(\kappa_l z_k\right), \quad k = 1,\ 2, \ldots,\ N, \tag{25}$$

where

$$T_l\left(\kappa_l z\right) = \begin{cases} -\frac{\mathrm{i}gA}{\omega} \sinh\left[\kappa_l\left(h-d\right)\right]\left[\kappa_l \cosh\left(\kappa_l z\right) + \nu \sinh\left(\kappa_l z\right)\right], & -d \le z \le 0 \\ -\frac{\mathrm{i}gA}{\omega}\left(\nu \cosh \kappa_l d - \kappa_l \sinh \kappa_l d\right) \cosh\left[\kappa_l\left(z+h\right)\right], & -h \le z \le -d \end{cases}.$$

Here, $\nu = \omega^2/g$, D_{nl}^k are unknown complex coefficients. The eigenvalues κ_l are the roots of:

$$\kappa_l\left[\frac{\omega^2}{g}\cosh\left(\kappa_l d\right) - \kappa_l \sinh\left(\kappa_l d\right)\right]\sinh\left[\kappa_l\left(h-d\right)\right] = \mathrm{i}\sigma_0\left[\frac{\omega^2}{g}\cosh\left(\kappa_l h\right) - \kappa_l \sinh\left(\kappa_l h\right)\right]$$

in the upper half complex plane of κ_l for $0 < \sigma_0 < +\infty$.

We could obtain the following linear equations by substituting Eqs. (24) and (25) into transmission conditions (18) and (19) and using the orthogonality of the vertical eigenfunction of the exterior region:

$$A_{mp}^k R_m'\left(k_p a\right) S_{pp} + \sum_{j=1, j\neq k}^{N} \sum_{n=-\infty}^{\infty} A_{np}^j Q_{n,-m}^{jk\prime}\left(k_p a\right) S_{pp} = \sum_{l=1}^{\infty} D_{ml}^k \kappa_l \frac{J_m'\left(\kappa_l a\right)}{J_m\left(\kappa_l a\right)} C_{pl} - I_k k_0 J_m'\left(k_0 a\right) e^{\mathrm{i}m\left(\frac{\pi}{2}-\beta\right)} S_{0p}, \tag{26}$$

$$A_{mp}^k R_m\left(k_p a\right) S_{pp} + \sum_{j=1, j\neq k}^{N} \sum_{n=-\infty}^{\infty} A_{np}^j Q_{n,-m}^{jk}\left(k_p a\right) S_{pp} = \sum_{l=1}^{\infty} D_{ml}^k \left[1 - \frac{\kappa_l J_m'\left(\kappa_l a\right)}{\mathrm{i}\sigma_1 J_m\left(\kappa_l a\right)}\right] C_{pl} - I_k J_m\left(k_0 a\right) e^{\mathrm{i}m\left(\frac{\pi}{2}-\beta\right)} S_{0p}. \tag{27}$$

Here, S_{pp}, S_{0p} and C_{pl} are integrals of the vertical eigenfunctions, and the results are presented in the appendix. The unknown coefficients can be obtained by combining the two linear equations.

The hydrodynamic forces and the water surface elevation surrounding the array of cylinders can be calculated using the derived velocity potentials.

The surge force of cylinder j can be calculated by:

$$F_j = \frac{a\omega\rho\pi}{\sigma_1}\left[\sum_{l=1}^{\infty} D_{1l}^j \kappa_l \frac{J_1'\left(\kappa_l a\right)}{J_1\left(\kappa_l a\right)} S_f + \sum_{l=1}^{\infty} D_{-1l}^j \kappa_l \frac{J_{-1}'\left(\kappa_l a\right)}{J_{-1}\left(\kappa_l a\right)} S_f\right]. \tag{28}$$

where S_f are integrals of $T_l\left(\kappa_l z\right)$ in the interval -h to 0. The result is also shown in the appendix.

The free-surface elevation is given by the linearized Bernoulli equation on z=0:

$$\eta = \frac{\mathrm{i}\omega\phi_k}{g}\Big|_{z=0},\ k = 0, 1, 2, \ldots,\ N. \tag{29}$$

4. Numerical results and discussions

In this section, the model of an isolated porous cylinder is calculated first. Then, a four-cylinders system illustrated in Figure 2 is calculated in order to investigate the diffraction phenomenon of an array of porous cylinders with porous plates fixed inside. The magnitudes of free-surface elevations and surge forces are nondimensionalized by $2A$ and $2\rho g A a^2 h$, respectively.

The dimensionless surge force of an isolated porous cylinder varies with the dimensionless wavenumber, as seen in Fig. 3. The calculation parameters are $h/a = 5$, $b_1 = 2\pi$, $d/h = 0.01$ and $b_0 = 1000.0,\ 20.0,\ 10.0,\ 5.0,\ 0.0001$. It should be noted that the circles represent the case without the plate, and the result is from Williams and Li (2000). It can be concluded from Fig. 3 that when $b_0 = 1000$, it can be regarded as the absence of the plate. The presence of a porous plate has little effect on the structure's surge force over the whole frequency range, as seen in this figure. Regardless of the permeability of the plate, the peak value of the surge force of an isolated porous cylinder remains unchanged.

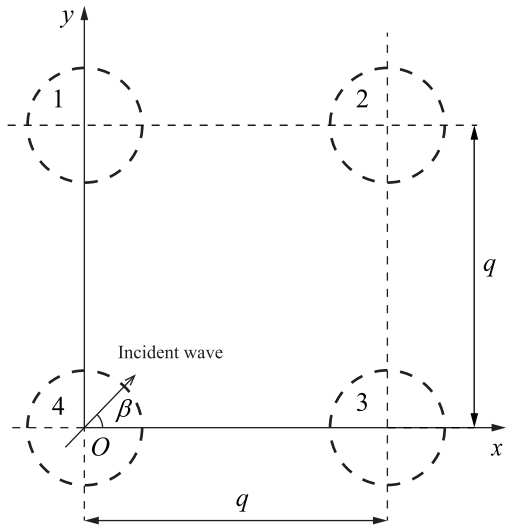

Fig. 2. Geometric model for a four-cylinders system.

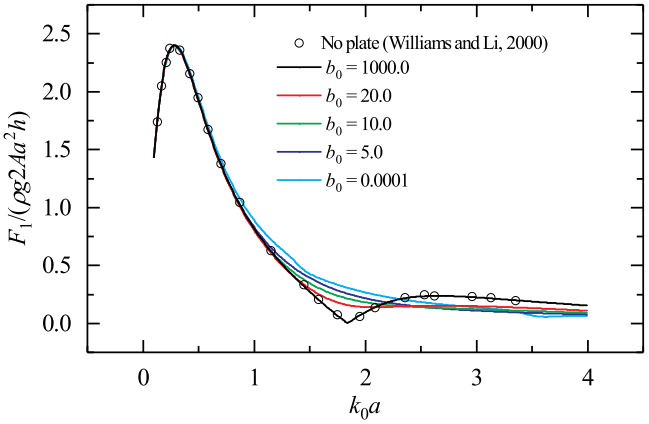

Fig. 3. Dimensionless surge force of an isolated porous cylinder with a porous plate fixed inside for $h/a = 5$, $b_1 = 2\pi$, $d/h = 0.01$ and $b_0 = 1000.0,\ 20.0,\ 10.0,\ 5.0,\ 0.0001$.

Fig. 4 shows the dimensionless wave run up on the exterior and interior walls of an isolated porous cylinder for $k_0a = 0.6$, $h/a = 5$, $b_1 = 2\pi$, $d/h = 0.01$ and $b_0 = 1000.0,\ 20.0,\ 10.0,\ 5.0,\ 0.0001$. The results of Williams and Li (2000) are recovered in Fig. 4. The presence of the plate, as shown in Fig. 4 (a), decreases the wave run up outside the cylinder. However, regardless of the permeability of the plate, the maximum point of wave run up outside the cylinder always occurs at $\theta = 180$. On the contrary, the maximum point of wave run up inside the cylinder occurs at $\theta = 0$ as illustrated in Fig. 4 (b). Meanwhile, as the permeability of the plate diminishes, the peak value of wave run up both inside and outside the cylinder gradually decreases.

Fig. 5 depicts the total surge force in the x-direction for $h/a = 5$, $q/a = 4$, $b_1 = 2\pi$, $\beta = 45$, $d/h = 0.01$ and $b_0 = 1000.0,\ 20.0,\ 10.0,\ 5.0,\ 0.0001$. The circles in this figure also represent the results of Williams and Li (2000) for an array of porous cylinders without porous plates fixed inside. The peak value of the total surge force of the four-cylinders system decreases slightly with the gradual decrease of b_0, as shown in Fig. 5. By contrast, in the high frequency region ($k_0a > 1.5$), with the gradual decrease of b_0, the total surge force of the four-cylinders system

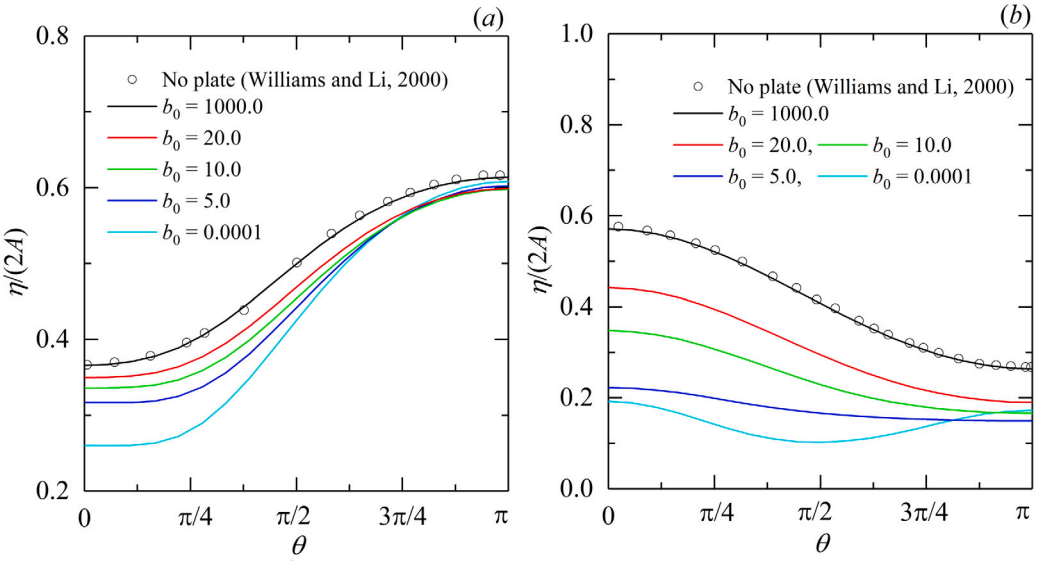

Fig. 4. Dimensionless wave run up on the exterior (a) and interior (b) walls of an isolated porous cylinder with a porous plate fixed inside for $k_0a = 0.6$, $h/a = 5$, $b_1 = 2\pi$, $d/h = 0.01$ and $b_0 = 1000.0,\ 20.0,\ 10.0,\ 5.0,\ 0.0001$.

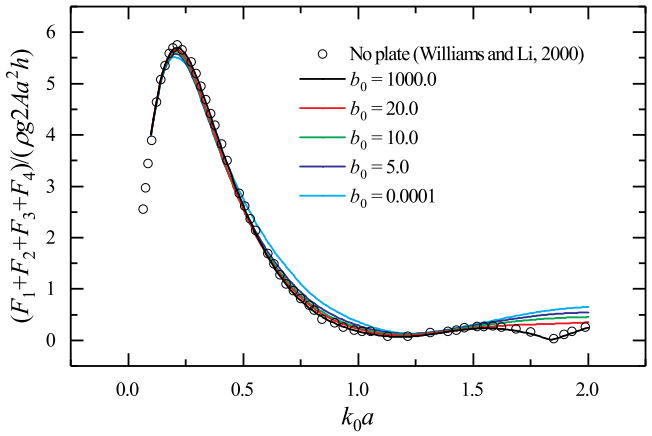

Fig. 5. Dimensionless surge force in the x-direction on a four-cylinder system for $h/a = 5$, $q/a = 4$, $b_1 = 2\pi$, $\beta = 45$, $d/h = 0.01$ and $b_0 = 1000.0,\ 20.0,\ 10.0,\ 5.0,\ 0.0001$.

increases slightly. In general, the existence of the plates has little effect on the total surge force of the four-cylinders system.

Figs. 6–7 show the dimensionless wave run up on each cylinder as an illustration of the effect of porosity on wave run up for $h/a = 5$, $q/a = 4$, $b_1 = 2\pi$, $\beta = 45$, $k_0a = \pi/2$, $d/h = 0.01$ and $b_0 = 1000.0,\ 20.0,\ 10.0,\ 5.0,\ 0.0001$. The results of Williams and Li (2000) are again recovered in Figs. 6–7. As can be seen from Fig. 6, the existence of the plates does not affect the position of the peak value of the wave run up outside the cylinders, that is, the upstream side. Except for cylinder 2, with the decrease of b_0, the peak value of wave run up on exterior wall increases gradually. For cylinder 2, the variation law of its peak point is just the opposite, which may be caused by the shielding effect of other cylinders. It can be concluded from Fig. 7 that the existence of the plates makes the wave run up on interior wall of the cylinder more complex. Meanwhile, it can be seen that the existence of the plates helps to reduce the wave run up on interior wall of the cylinder.

The influence of permeability on the dimensionless wave height in the vicinity of the four-cylinders system are presented in Figs. 8–10 for $h/a = 5$, $q/a = 4$, $d/h = 0.01$, $b_1 = 2\pi$, $\beta = 45$, $k_0a = \pi/2$ and $b_0 = 0.0001,\ 10.0,\ 10000.0$. These three pictures show the influence of the porous plates on the diffraction of the incident wave field. With the decrease of b_0, the setdown phenomenon of the free surface elevation on the downstream side of the system becomes more and more obvious. Even if the dimensionless porous effect parameter b_0 decreased to 0.0001, the wave focusing process mentioned by Yu and Chwang (1993) and Chwang and Wu (1994) was not observed in the system.

These results demonstrate the effect of the plates on the diffraction process of the porous cylinders, while differences in the effect of porous and impermeable plates on this process can also be found.

For a porous cylinder with a porous plate fixed inside, the process of the fluid passing through the plate consumes part of the wave energy and reduces the wave run up inside the cylinder. The porous plates with different permeability hardly change the trend of the wave run up curve inside the cylinder (Fig. 4 (b) and 7). For a porous cylinder with an impermeable plate ($b_0 = 0.0001$) fixed inside, the presence of the plate also reduces the wave run up inside the cylinder, but its effect on the wave run up is different from the effect of the porous plate on it (Fig. 7). Due to the phase interaction between the flows over and below the impermeable plates, the plates may cause wave trapping over the plates, including refraction and reflection (Chwang and Wu, 1994). The porous cylinder reduces the fluid entering the interior regions, easing wave trapping and avoiding the wave energy focusing.

The diffraction process becomes more complex due to the interaction of the plates in the array. Numerous calculations have shown that the impermeable plates may increase the peak value of wave run up outside some cylinders in the array (Cylinders 1, 3 and 4 in Fig. 6). Cylinder 2 is affected by the shielding effect of cylinders 1, 3 and 4, and the intense process of wave transformation above the plates is slowed down, resulting in a gradual decrease of the peak value of wave run up outside the cylinder with the decrease of the plate's permeability (Cylinder 2 in Fig. 6). This shielding effect is more obvious in Figs. 8–10. In this four-cylinders model, the combination of porous plates and porous cylinders can be regarded as a wave absorber with stronger wave absorption ability.

5. Conclusions

The interaction of water wave and an array of porous cylinders with porous plates fixed inside is investigated theoretically. An analytical solution has been established using the eigenfunction expansion approach under the assumptions of potential flow and linear wave theory. The correctness of the theory is verified by the published calculation

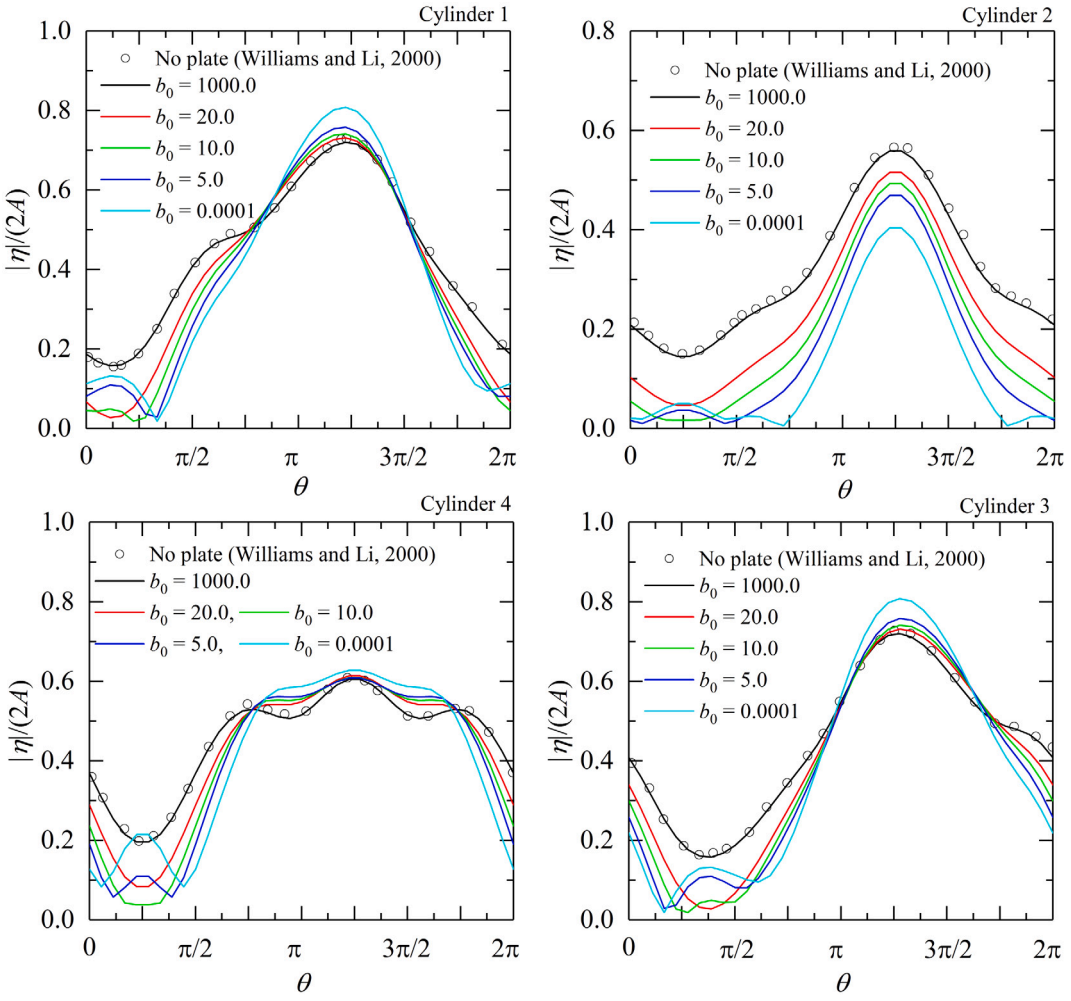

Fig. 6. Dimensionless wave run up on exterior wall of each cylinder of a four-cylinders system for $h/a = 5$, $q/a = 4$, $b_1 = 2\pi$, $\beta = 45$, $k_0 a = \pi/2$, $d/h = 0.01$ and $b_0 = 1000.0,\ 20.0,\ 10.0,\ 5.0,\ 0.0001$.

results of limiting cases. Then, numerical calculations are carried out for the four-cylinders system. The results reveal that the existence of the plate hardly affects the surge force of porous cylinder array, but it will significantly reduce the wave run up inside the cylinder. Meanwhile, the porous plates will also enhance the setdown phenomenon of the free surface elevation on the downstream side of the array, showing the wave absorption ability of the combined application of the porous plates and the porous cylinders.

CRediT authorship contribution statement

GuangYuan Wang: Conceptualization, Methodology. **MoHan Zhang:** Software, Data curation, Writing – original draft. **HuaQing Zhang:** Validation, Supervision, Writing – review & editing. **FaJun Yu:** Writing – review & editing.

Declaration of competing interest

The authors declare that they have no known competing financial interests or personal relationships that could have appeared to influence the work reported in this paper.

Acknowledgment

This work was supported by Chinese Academy of Science under Projects No. XDA22040203.

Appendix

The integral results used to solve the system of linear equations as shown in (26)–(27), are provided as follows:

$$S_{qp} = \int_{-h}^{0} Z_q(k_q z) Z_p(k_p z)\, dz = \begin{cases} -\left(\frac{gA}{\omega}\right)^2 \frac{1}{\cosh^2(k_0 h)} \left[\frac{h}{2} + \frac{\sinh(2k_0 h)}{4k_0}\right], & q = p = 0 \\ -\left(\frac{gA}{\omega}\right)^2 \frac{1}{\cos^2(k_p h)} \left[\frac{h}{2} + \frac{\sin(2k_p h)}{4k_p}\right], & q = p \geq 1 \\ 0, & q \neq p \end{cases} \tag{A.1}$$

$$\begin{aligned} C_{0l} &= \int_{-h}^{0} Z_0(k_0 z) T_l(\kappa_l z)\, dz \\ &= -\frac{g^2 A^2 \left[\nu \cosh(\kappa_l d) - \kappa_l \sinh(\kappa_l d)\right]}{\omega^2 \cosh(k_0 h)} \left\{ \frac{\sinh\left[(k_0 + \kappa_l)(h - d)\right]}{2(k_0 + \kappa_l)} \right. \\ &\quad \left. + \frac{\sinh\left[(k_0 - \kappa_l)(h - d)\right]}{2(k_0 - \kappa_l)} \right\} \\ &\quad - \frac{g^2 A^2 \kappa_l \sinh\left[\kappa_l (h - d)\right]}{\omega^2 \cosh(k_0 h)} \frac{\sinh(k_0 h) - \sinh\left[-d(k_0 + \kappa_l) + k_0 h\right]}{2(k_0 + \kappa_l)} \\ &\quad + \frac{g^2 A^2 \kappa_l \sinh\left[\kappa_l (h - d)\right]}{\omega^2 \cosh(k_0 h)} \frac{\sinh(k_0 h) + \sinh\left[-d(\kappa_l - k_0) - k_0 h\right]}{2(\kappa_l - k_0)} \end{aligned}$$

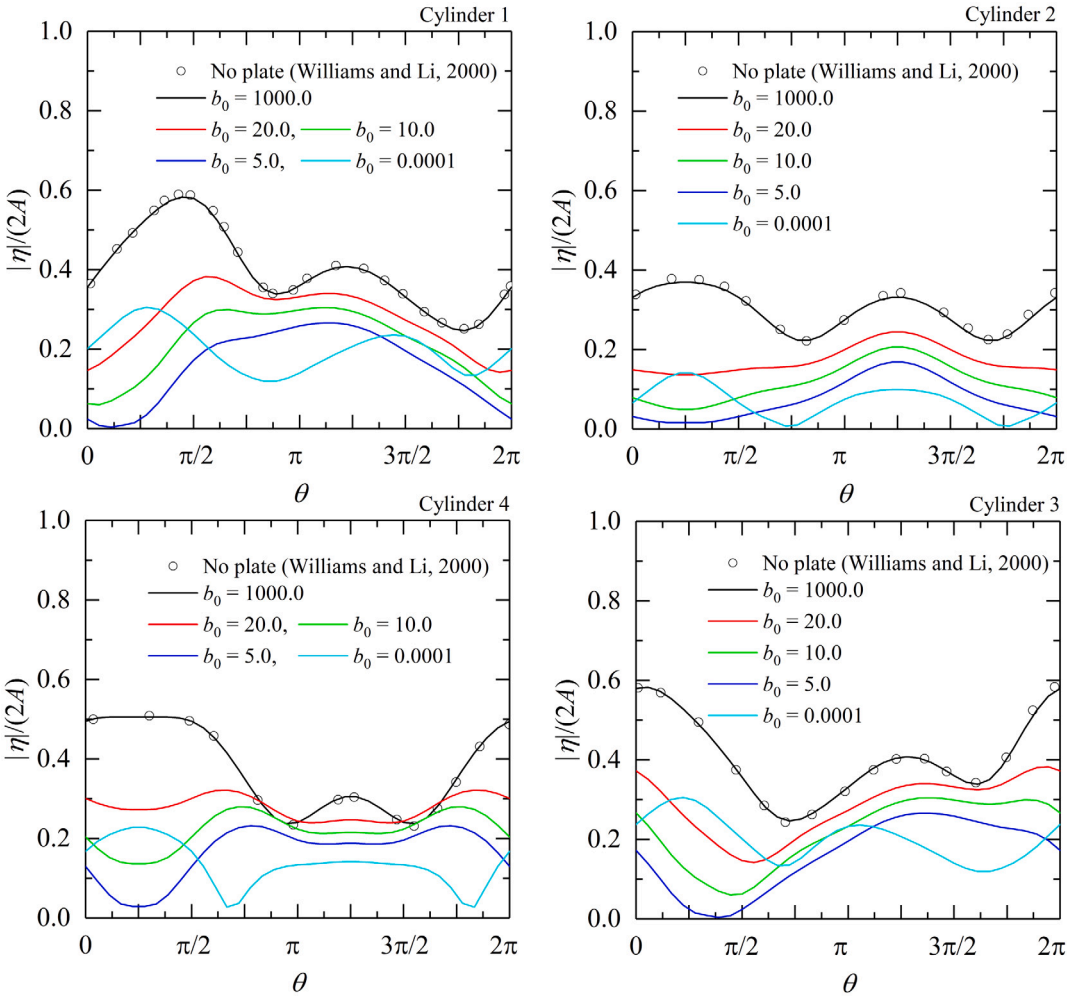

Fig. 7. Dimensionless wave run up on interior wall of each cylinder of a four-cylinders system for $h/a = 5$, $q/a = 4$, $b_1 = 2\pi$, $\beta = 45$, $k_0a = \pi/2$, $d/h = 0.01$ and $b_0 = 1000.0,\ 20.0,\ 10.0,\ 5.0,\ 0.0001$.

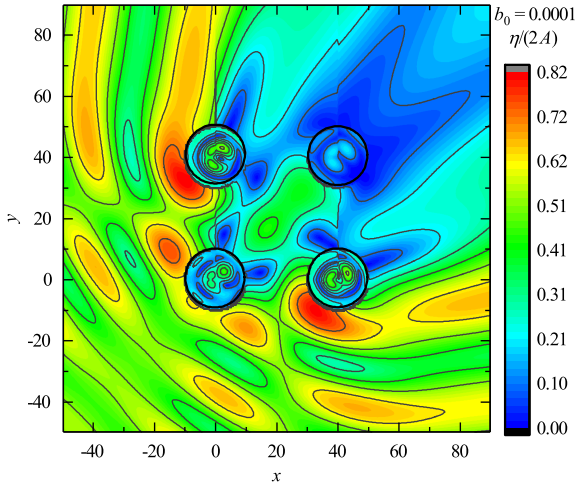

Fig. 8. Free surface elevations for the four-cylinders system for $h/a = 5$, $d/h = 0.01$, $q/a = 4$, $b_1 = 2\pi$, $\beta = 45$, $k_0a = \pi/2$ and $b_0 = 0.0001$.

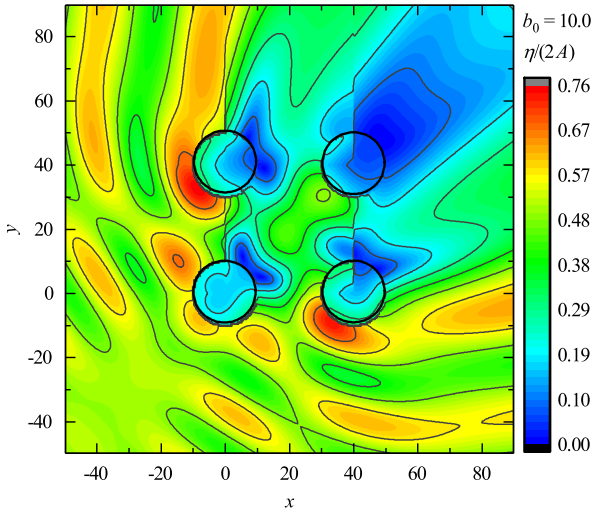

Fig. 9. Free surface elevations for the four-cylinders system for $h/a = 5$, $d/h = 0.01$, $q/a = 4$, $b_1 = 2\pi$, $\beta = 45$, $k_0a = \pi/2$ and $b_0 = 10.0$.

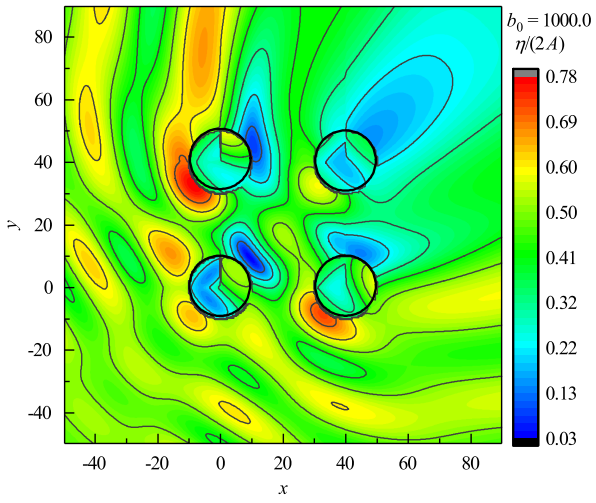

Fig. 10. Free surface elevations for the four-cylinders system for $h/a = 5$, $d/h = 0.01$, $q/a = 4$, $b_1 = 2\pi$, $\beta = 45$, $k_0 a = \pi/2$ and $b_0 = 1000.0$.

$$
\begin{aligned}
&- \frac{g^2 A^2 \nu \sinh\left[\kappa_l (h-d)\right]}{\omega^2 \cosh\left(k_0 h\right)} \frac{\cosh\left(k_0 h\right) - \cosh\left[-d\left(\kappa_l + k_0\right) + k_0 h\right]}{2\left(\kappa_l + k_0\right)} \\
&- \frac{g^2 A^2 \nu \sinh\left[\kappa_l (h-d)\right]}{\omega^2 \cosh\left(k_0 h\right)} \frac{\cosh\left(k_0 h\right) - \cosh\left[-d\left(\kappa_l - k_0\right) - k_0 h\right]}{2\left(\kappa_l - k_0\right)},
\end{aligned}
\tag{A.2}
$$

$$
\begin{aligned}
C_{pl} &= \int_{-h}^{0} Z_p\left(k_p z\right) T_l\left(\kappa_l z\right) dz, \ p > 0 \\
&= -\frac{g^2 A^2 \kappa_l \left[\nu \cosh\left(\kappa_l d\right) - \kappa_l \sinh\left(\kappa_l d\right)\right] \sinh\left[\kappa_l (h-d)\right] \cos\left[k_p (h-d)\right]}{\omega^2\left(\kappa_l^2 + k_p^2\right)\cos\left(k_p h\right)} \\
&- \frac{g^2 A^2 k_p \left[\nu \cosh\left(\kappa_l d\right) - \kappa_l \sinh\left(\kappa_l d\right)\right] \cosh\left[\kappa_l (h-d)\right] \sin\left[k_p (h-d)\right]}{\omega^2\left(\kappa_l^2 + k_p^2\right)\cos\left(k_p h\right)} \\
&- \frac{g^2 A^2 \kappa_l \sinh\left[\kappa_l (h-d)\right]}{\omega^2\left(\kappa_l^2 + k_p^2\right)\cos\left(k_p h\right)} \left\{k_p \sin\left(k_p h\right) + \kappa_l \sinh\left(\kappa_l d\right) \cos\left[k_p (h-d)\right]\right\} \\
&+ \frac{g^2 A^2 \kappa_l \sinh\left[\kappa_l (h-d)\right]}{\omega^2\left(\kappa_l^2 + k_p^2\right)\cos\left(k_p h\right)} k_p \cosh\left(\kappa_l d\right) \sin\left[k_p (h-d)\right] \\
&- \frac{g^2 A^2 \nu \sinh\left[\kappa_l (h-d)\right]}{\omega^2\left(\kappa_l^2 + k_p^2\right)\cos\left(k_p h\right)} \left\{\kappa_l \cos\left(k_p h\right) - \kappa_l \cosh\left(\kappa_l d\right) \cos\left[k_p (h-d)\right]\right\} \\
&- \frac{g^2 A^2 \nu \sinh\left[\kappa_l (h-d)\right]}{\omega^2\left(\kappa_l^2 + k_p^2\right)\cos\left(k_p h\right)} \left\{k_p \sinh\left(\kappa_l d\right) \sin\left[k_p (h-d)\right]\right\}.
\end{aligned}
\tag{A.3}
$$

The integral used to derive the surge force is shown in (28), as follows:

$$
\begin{aligned}
S_f &= \int_{-h}^{0} T\left(\kappa_l z\right) dz \\
&= \frac{\mathrm{i} g A \left[\nu \cosh\left(\kappa_l d\right) - \kappa_l \sinh\left(\kappa_l d\right)\right] \sinh\left[\kappa_l (d-h)\right]}{\omega \kappa_l} \\
&- \frac{\mathrm{i} g A \sinh\left[\kappa_l (h-d)\right] \sinh\left(\kappa_l d\right)}{\omega} \\
&+ \frac{\mathrm{i} g A \nu \sinh\left[\kappa_l (h-d)\right] \left[\cosh\left(\kappa_l d\right) - 1\right]}{\omega \kappa_l}.
\end{aligned}
\tag{A.4}
$$

References

Abramowitz, M., Stegun, I.A., 1964. Handbook of mathematical functions with formulas, graphs, and mathematical tables, Vol. 55. US Government printing office.

Bao, W., Zhao, F., Kinoshita, T., 2009. Calculation of wave forces acting on a cylinder with a porous plate fixed inside. In: International Conference on Offshore Mechanics and Arctic Engineering, Vol.43444, pp. 1253–1260.

Cho, I., Kim, M., 2000. Interactions of horizontal porous flexible membrane with waves. J. Waterw. Port Coast. Ocean Eng. 126 (5), 245–253.

Cho, I., Kim, M., 2008. Wave absorbing system using inclined perforated plates. J. Fluid Mech. 608, 1–20.

Cho, I., Kim, M., 2013. Transmission of oblique incident waves by a submerged horizontal porous plate. Ocean Eng. 61, 56–65.

Chwang, A.T., Wu, J., 1994. Wave scattering by submerged porous disk. J. Eng. Mech. 120 (12), 2575–2587.

Darwiche, M., Williams, A., Wang, K.-H., 1994. Wave interaction with semiporous cylindrical breakwater. J. Waterw. Port Coast. Ocean Eng. 120 (4), 382–403.

Evans, D.V., Peter, M.A., 2011. Asymptotic reflection of linear water waves by submerged horizontal porous plates. J. Eng. Math. 69 (2–3), 135–154.

Kagemoto, H., Yue, D.K., 1986. Interactions among multiple three-dimensional bodies in water waves: an exact algebraic method. J. Fluid Mech. 166, 189–209.

Linton, C., Evans, D., 1990. The interaction of waves with arrays of vertical circular cylinders. J. Fluid Mech. 215, 549–569.

Liu, Y., Li, Y.-c., 2011. An alternative analytical solution for water-wave motion over a submerged horizontal porous plate. J. Eng. Math. 69 (4), 385–400.

Liu, Y., Li, H.-j., Li, Y.-c., He, S.-y., 2011. A new approximate analytic solution for water wave scattering by a submerged horizontal porous disk. Appl. Ocean Res. 33 (4), 286–296.

Liu, Y., Li, Y.-c., Teng, B., 2007. Wave interaction with a perforated wall breakwater with a submerged horizontal porous plate. Ocean Eng. 34 (17–18), 2364–2373.

Liu, Y., Li, Y.-c., Teng, B., Dong, S., 2008. Wave motion over a submerged breakwater with an upper horizontal porous plate and a lower horizontal solid plate. Ocean Eng. 35 (16), 1588–1596.

Maniar, H., Newman, J., 1997. Wave diffraction by a long array of cylinders. J. Fluid Mech. 339, 309–330.

Molin, B., Nielsen, F., et al., 2004. Heave added mass and damping of a perforated disk below the free surface. In: Proceedings of the 19th International Workshop on Water Waves and Floating Bodies, Cortona, Italy.

Sankarbabu, K., Sannasiraj, S., Sundar, V., 2007. Interaction of regular waves with a group of dual porous circular cylinders. Appl. Ocean Res. 29 (4), 180–190.

Spring, B.H., Monkmeyer, P.L., 1974. Interaction of plane waves with vertical cylinders. Coast. Eng. Proc. 1 (14), 107.

Taylor, G.I., 1956. Fluid flow in regions bounded by porous surfaces. Proc. R. Soc. Lond. Series A. Math. Phys. Sci. 234 (1199), 456–475.

Walker, D.A., Taylor, R.E., 2005. Wave diffraction from linear arrays of cylinders. Ocean Eng. 32 (17–18), 2053–2078.

Wang, K.-H., Ren, X., 1994. Wave interaction with a concentric porous cylinder system. Ocean Eng. 21 (4), 343–360.

Wang, G., Yu, F., Zhang, H., Zhang, E., Li, Z., 2021. Wave diffraction from a concentric truncated cylinder system with a porous ring plate fixed inside. Ocean Eng. 228, 108932.

Williams, A., Li, W., 1998. Wave interaction with a semi-porous cylindrical breakwater mounted on a storage tank. Ocean Eng. 25 (2–3), 195–219.

Williams, A., Li, W., 2000. Water wave interaction with an array of bottom-mounted surface-piercing porous cylinders. Ocean Eng. 27 (8), 841–866.

Wu, J., Chwang, A.T., 2002. Wave diffraction by a vertical cylinder with a porous ring plate. J. Eng. Mech. 128 (2), 164–171.

Yip, T.L., Chwang, A.T., 1998. Water wave control by submerged pitching porous plate. J. Eng. Mech. 124 (4), 428–434.

Yu, X., Chwang, A.T., 1993. Analysis of wave scattering by submerged circular disk. J. Eng. Mech. 119 (9), 1804–1817.

Zeng, X., Yu, F., Shi, M., Wang, Q., 2019. Fluctuation of magnitude of wave loads for a long array of bottom-mounted cylinders. J. Fluid Mech. 868, 244–285.

Zhao, F., Bao, W., Kinoshita, T., Itakura, H., 2010. Interaction of waves and a porous cylinder with an inner horizontal porous plate. Appl. Ocean Res. 32 (2), 252–259.

Zhao, F., Zhang, T., Wan, R., Huang, L., Wang, X., Bao, W., 2017. Hydrodynamic loads acting on a circular porous plate horizontally submerged in waves. Ocean Eng. 136, 168–177.